IEEE Access
Multidisciplinary ⋮ Rapid Review ⋮ Open Access Journal

Received March 9, 2021, accepted March 21, 2021, date of publication March 31, 2021, date of current version July 14, 2021.

Digital Object Identifier 10.1109/ACCESS.2021.3069885

Coexisting Multiple Attractors in a Fourth Order Chua's Circuit With Experimental Verifications by Analog and Digital Circuits

LEI ZHU [1,2] AND MINGHAI PAN [1]

[1]College of Electronic and Information Engineering, Nanjing University of Aeronautics and Astronautics, Nanjing 211106, China
[2]College of Electrical and Information Engineering, Jiangsu University of Technology, Changzhou 213001, China

Corresponding author: Minghai Pan (panmh@nuaa.edu.cn)

This work was supported by the National Natural Science Foundation of China under Grant 61271327.

ABSTRACT Exploring coexistence of multiple attractors brought by the multistability for circuits and systems has a significant meaning in the theoretical researches and practical applications for chaos. In this article, a succinct fourth order Chua's circuit is proposed by replacing the negative resistance with an ordinary positive resistance in a traditional fourth order one. The two-dimensional stability analysis for equilibrium points shows that this circuit possesses one unstable saddle-focus point with index 1 and two stable node-focus points. Coexisting bifurcation models, multiple attractors and the corresponding attraction basins are revealed by a series of numerical simulations. The clear crisis scenario of the coexisting limit cycles of period-3 bridging the coexisting single-scroll attractors of chaos and the double-scroll one is observed by the bifurcation analyses. The dual-mode experimental verifications by the analog and digital circuits are carried out on the self-made printed circuit boards, which validate the simulated dynamical behaviors with the combination of physics and engineering.

INDEX TERMS Succinct fourth order Chua's circuit, multiple attractors, crisis scenario, dual-mode experimental verifications, microcontroller.

I. INTRODUCTION

Chaos is an important interdisciplinary research theme in the field of mathematics, physics, and engineering [1]. In recent years, the study for multistability [2], [3] and even extreme multistability [4]–[6] in the chaotic system has become a hot spot, where the coexisting bifurcation models and multiple attractors [7], [8] can be observed by numerical simulation or experimental measurement. As a study focus among the nonlinear circuits, the classical third order Chua's circuit [9], [10] demonstrates the chaos phenomenon perfectly in theory and practice [11], [12]. On the basis of this classical circuit, the various forms of generalized Chua's circuits and systems [13]–[26] build a deep recognition of chaos for the academia further. In these studies, the new features such as stable equilibrium points [14]–[17], multi-scroll attractors [18]–[21], multiple attractors [17], multiple scroll coexisting attractors [22], SC-CNN-based mode [23] and inductorless implementation approaches [24]–[26] have been revealed in succession. The fourth order Chua's circuit is also a form of generalized Chua's circuit, yet the related reports are not often noticed. In 2020 [27], a fourth order Chua's circuit is obtained by concatenating a parallel resistance-capacitance network with the inductance in the classical third order Chua's circuit, where the double-scroll attractor, coexisting single-scroll attractors and limit cycles brought by period-doubling bifurcation mechanism can be found. Similar to the classical Chua's circuit, this fourth order circuit possesses three unstable saddle-focus points. In 2004 [28], a fourth order Chua's circuit was constructed via concatenating an additional inductance with the resistance in the classical Chua's circuit. And at the same time a parallel negative resistance was added to the LC parallel resonance in this fourth order Chua's circuit. Under this circuit construction, chaotic [28], hyperchaotic [28] and periodic bursting [29] oscillation behaviors were discovered. Yet the physical implementation of a negative resistance needs to adopt an op amp [17], which increases the complexity of the hardware circuit. Obviously,

The associate editor coordinating the review of this manuscript and approving it for publication was Sun Junwei.

it is meaningful for chaotic circuit to simplify the physical implementation [30]. On the other hand, a valuable question is whether a fourth order Chua's circuit can generate multistability phenomenon. For these two factors, a succinct fourth order Chua's circuit is presented in the article, where an ordinary positive resistance is used to replace the negative one in the traditional fourth order Chua's circuit [28]. Accordingly, the features of stable equilibrium points and multiple attractors are discovered in this new circuit, thus enriching our awareness to fourth order Chua's circuit.

For validating the basic physical realizability of chaotic circuit, experimental verification by analog circuit is often a necessary step during the course of study. However, due to the influences from the objective factors such as the parasitic parameters of electronic components and the detection capability of the instruments, sometimes the success for analog circuit experiment is hardly guaranteed. Obviously, sufficient verification is the fundamental guarantee of the correctness for the theoretical study. Therefore, it is meaningful to introduce the verification mode of digital circuit to overcome this inadequacy of analog circuit. Besides, the reliable engineering realizability by digital circuit offers great convenience to the industrial applications of chaos. With the development of digital electronic technology, the microcontroller is effectively introduced into discrete chaotic map [31], and even continuous chaotic systems [32]–[34]. Based on these, a type of 16-bit microcontroller MSP430F5438A with low power consumption is used for the design of digital circuit in this article, which forms the dual-mode experimental verifications for the new chaotic circuit together with the analog circuit.

The rest of this article is organized as follows. In Section II, the new succinct fourth order Chua's circuit is established. The corresponding stability of equilibrium is discussed, ranging from the normalized typical parameters to two-parameter plane. In Section III, the analysis of multi-stable dynamics for this new circuit is carried out by a series of numerical computation. In Section IV, the design schemes and the test results of dual-mode experiments with analog and digital circuits are expounded. In the end, some conclusions are given by Section V.

II. THE SUCCINCT FOURTH ORDER CHUA'S CIRCUIT

In this section, the succinct fourth order Chua's circuit is proposed and the corresponding mathematical model is deduced. Through the variable substitutions and parameter transformations, a normalized model is derived further. The corresponding stability of equilibrium points is discussed, ranging from the normalized typical parameters to two-parameter plane.

A. CIRCUIT STRUCTURE AND STATE EQUATIONS

The new succinct fourth order Chua's circuit is drawn in **Fig. 1**, where an op amp and ten passive elements are applied. The unit linked with blue color is a reduced piecewise-linear Chua's diode, which is obtained through a negative impedance converter (NIC) [24], [35]. Compared to the

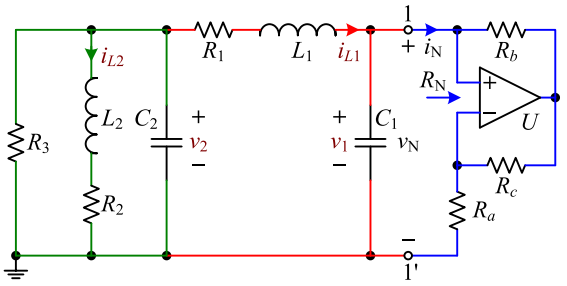

FIGURE 1. The constitution of the new circuit.

fourth order Chua's circuit reported by [28], the adoption of positive resistance instead of negative one for R_3 simplify the circuit and cut down the cost. At the same time, the equivalent series resistance (ESR) of the inductance L_2 is considered, a low resistance R_2 is introduced to this circuit. The physical behaviors of the circuit can be represented by four state variables of v_1, v_2, i_{L1}, and i_{L2} corresponding to four dynamic elements.

To nonlinear component R_N, the mathematical relationship for v_N and i_N can be expressed as [24]

$$i_N = f(v_N) = S_b v_N + \frac{1}{2}(S_a - S_b)(|v_N + E_P| - |v_N - E_P|) \tag{1}$$

By setting $R_b = R_c$, the parameter transformation relations can be derived as

$$S_a = -\frac{1}{R_a}, \quad S_b = \frac{1}{R_b}, \quad E_P = \frac{R_a}{R_a + R_b} E_{sat} \tag{2}$$

Here E_{sat} stands for the output saturation voltage of amplifier U.

For a fourth order chaotic circuit, four coupled ordinary differential equations about corresponding state variables can be established. According to the laws of Kirchhoff, the mathematical model for the circuit shown in **Fig. 1** is deduced as

$$\begin{cases} C_1 \dfrac{dv_1}{dt} = i_{L1} - f(v_1) \\ C_2 \dfrac{dv_2}{dt} = -\dfrac{v_2}{R_3} - i_{L1} - i_{L2} \\ L_1 \dfrac{di_{L1}}{dt} = v_2 - v_1 - R_1 i_{L1} \\ L_2 \dfrac{di_{L2}}{dt} = v_2 - R_2 i_{L2} \end{cases} \tag{3}$$

where the nonlinear function $f(v_1)$ is denoted with (1).

B. NORMALIZED MODEL AND STABILITY OF EQUILIBRIUM POINTS

To simplify the analysis, a series of variable substitutions and parameter transformations are introduced, as listed by

$$\begin{aligned} &x = v_1/E_P, \quad y = v_2/E_P, \quad z = R_1 i_{L1}/E_P, \quad w = R_1 i_{L2}/E_P, \\ &\tau = t/(R_1 C_2), \quad \alpha_1 = C_2/C_1, \quad \alpha_2 = R_1/R_3, \quad \alpha_3 = R_2/R_1, \\ &\beta_1 = R_1^2 C_2/L_1, \quad \beta_2 = R_1^2 C_2/L_2, \quad m_a = S_a R_1, \quad m_b = S_b R_1 \end{aligned} \tag{4}$$

Thus model (3) is reconstructed as a normalized form, as given by

$$\begin{cases} \dot{x} = \alpha_1 [z - F(x)] \\ \dot{y} = -\alpha_2 y - z - w \\ \dot{z} = \beta_1 (y - x - z) \\ \dot{w} = \beta_2 (y - \alpha_3 w) \end{cases} \tag{5}$$

where the dimensionless piecewise-linear function $F(x)$ is represented as

$$F(x) = m_b x + \frac{1}{2}(m_a - m_b)(|x+1| - |x-1|) \tag{6}$$

Different from some chaotic systems with infinite equilibria [6] and even line equilibrium [4] based on nonlinear component memristor [36], the fourth order Chua's circuit has finite equilibrium points. Aimed at normalized model (5), three equilibrium points can be achieved through algebraic computation, as expressed by

$$\begin{cases} Q_0 = (0, 0, 0, 0) \\ Q_\pm = (\pm(1 + \alpha_2\alpha_3 + \alpha_3)k, \pm\alpha_3 k, \mp(1 + \alpha_2\alpha_3)k, \pm k) \end{cases} \tag{7}$$

Here $k = (m_b - m_a)/[(1 + \alpha_2\alpha_3 + \alpha_3)(m_b + 1) - \alpha_3]$ and it's easy to see that Q_+ and Q_- are symmetrical about origin of coordinates.

Accordingly, the Jacobi matrix of Eq. (5) on the three equilibrium points (7) is calculated as

$$\mathbf{J}(c) = \begin{bmatrix} -\alpha_1 c & 0 & \alpha_1 & 0 \\ 0 & -\alpha_2 & -1 & -1 \\ -\beta_1 & \beta_1 & -\beta_1 & 0 \\ 0 & \beta_2 & 0 & -\beta_2\alpha_3 \end{bmatrix} \tag{8}$$

where $c = m_a$ for Q_0 and $c = m_b$ for $Q_\pm$. The secular equation for matrix (8) on these equilibrium points can be represented as

$$P(\lambda) = \lambda^4 + a_1\lambda^3 + a_2\lambda^2 + a_3\lambda + a_4 = 0 \tag{9}$$

where

$$\begin{aligned} a_1 &= \alpha_1 c + \alpha_2 + \alpha_3\beta_2 + \beta_1 \\ a_2 &= \alpha_1\beta_1(1 + c) + (\alpha_1 c + \beta_1)(\alpha_2 + \alpha_3\beta_2) \\ &\quad + \alpha_2\alpha_3\beta_2 + \beta_1 + \beta_2 \\ a_3 &= (\alpha_1 c + \beta_1)(\alpha_2\alpha_3\beta_2 + \beta_2) \\ &\quad + \alpha_1\beta_1(1 + c)(\alpha_2 + \alpha_3\beta_2) + \beta_1(\alpha_1 c + \alpha_3\beta_2) \\ a_4 &= \alpha_1\beta_1\beta_2[(1 + c)(1 + \alpha_2\alpha_3) + \alpha_3 c] \end{aligned} \tag{10}$$

To the circuit given in **Fig. 1**, the typical parameters of the discrete components are listed as $R_a = 1.8$ kΩ, $R_b = R_c = 20$ kΩ, $R_1 = 1.9$ kΩ, $R_2 = 10$ Ω, $R_3 = 20$ kΩ, $C_1 = 5.8$ nF, $C_2 = 55$ nF, $L_1 = 2$ mH, $L_2 = 20$ mH. According to parameter transformations in (4), the normalized typical parameters can be calculated as

$$\begin{aligned} &\alpha_1 = 9.482759, \quad \alpha_2 = 0.095, \quad \alpha_3 = 0.008947368, \\ &\beta_1 = 99.275, \quad \beta_2 = 9.9275, \\ &m_a = -1.055556, \quad m_b = 0.095 \end{aligned} \tag{11}$$

By endowing system's initial states $(x(0), y(0), z(0), w(0))$ with different values, the phase portraits for model (5) in $x - y$ plane are simulated by MATLAB ode23 algorithm with normalized parameters (11), as given by **Fig. 2.** It can be concluded that four coexisting attractors including double-scroll attractor of chaos, the limit cycle with large amplitude, left-right point attractors can be triggered with appropriate initial values.

Under normalized typical parameters (11), the specific results for equilibrium points (7) can be achieved as

$$\begin{cases} \bar{Q}_0 = (0, 0, 0, 0) \\ \bar{Q}_\pm = (\pm 1.059308, \pm 0.009386, \mp 1.049922, \pm 1.04903) \end{cases} \tag{12}$$

The corresponding eigenvalues related to these three equilibrium points can be calculated numerically from **Eq. (9)**, as listed by

$$\begin{aligned} \bar{Q}_0 : \lambda_1 &= 1.8298, \quad \lambda_2 = -88.609, \\ \lambda_{3,4} &= -1.3351 \pm \mathrm{j}1.4025 \\ \bar{Q}_\pm : \lambda_{1,2} &= -0.1634 \pm \mathrm{j}3.0254, \quad \lambda_3 = -87.2328, \\ \lambda_4 &= -12.8002 \end{aligned} \tag{13}$$

Thus, $\bar{Q}_0$ is one unstable saddle-focus point of index 1 with only one positive real part for all the four corresponding eigenvalues [37], [38] and $\bar{Q}_\pm$ are two stable node-focus points. The numerical analysis indicates that these features of stability for equilibrium points Q_0 and $Q_\pm$ can be found in a large scale of parameters. On the basis of normalized typical parameters (11), when the parameter α_1 varies from 8.2 to 9.75 and β_2 varies from 9 to 10.5, the maximum value spectrum for the real parts of four eigenvalues related to the equilibrium points Q_0 and $Q_\pm$ are drawn by **Fig. 3** (a1) and (a2) respectively. Similarly, when the parameter α_2 varies from 0.05 to 0.3 and β_1 varies from 80 to 120, the maximum value spectrum for the real parts of four eigenvalues are drawn by **Fig. 3** (b1) and (b2) respectively.

III. THE ANALYSIS OF MULTI-STABLE DYNAMICS

In this section, coexisting bifurcation models, multiple attractors and the corresponding attraction basins are revealed by a series of numerical computation. Further, two-parameter dynamical behaviors are analyzed in the parameter planes corresponding to **Fig. 3**. Thus, the two effects from the parameters and the initial values for this circuit are discussed in a comprehensive way.

A. COEXISTING BIFURCATION MODELS AND MULTIPLE ATTRACTORS

According to the results in **Section II**, the dynamical behaviors to the new fourth order circuit are obviously sensitive about initial values. By endowing system's initial states $(x(0), y(0), z(0), w(0))$ with five groups of values, the corresponding

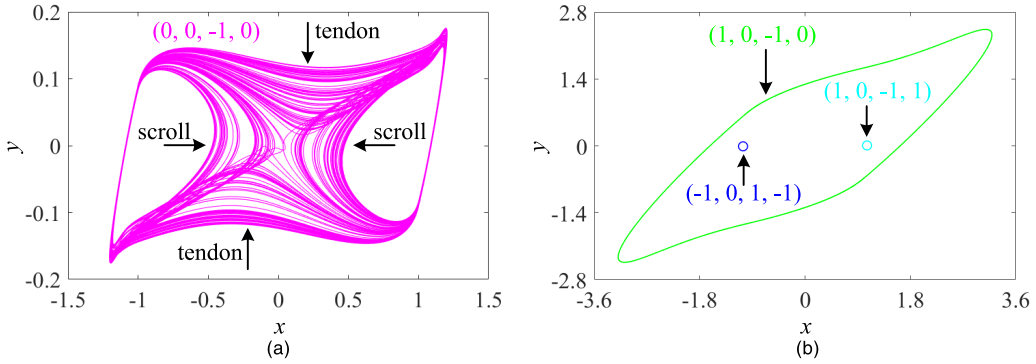

FIGURE 2. The phase portraits with normalized parameters. (a) the double-scroll chaotic attractor under $(x(0), y(0), z(0), w(0)) = (0, 0, -1, 0)$, (b) the limit cycle with large amplitude, left-right point attractors under $(x(0), y(0), z(0), w(0)) = (1, 0, -1, 0), (-1, 0, 1, -1), (1, 0, -1, 1)$.

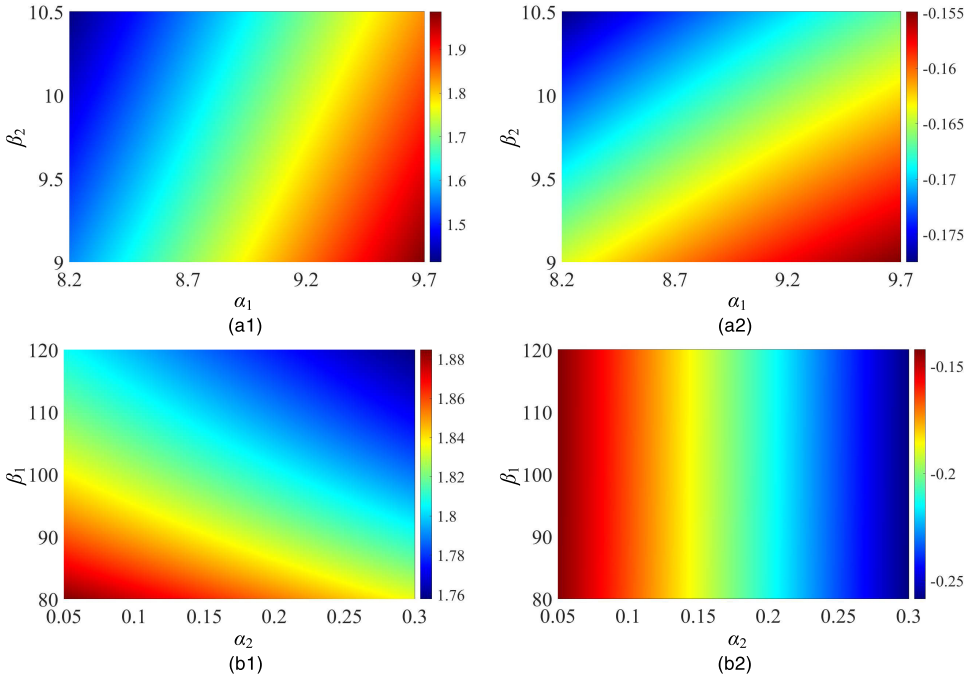

FIGURE 3. The graphical maximum value spectrum for the real parts of four eigenvalues related to the equilibrium points Q_0 and $Q_\pm$. (a1) the equilibrium point Q_0 under the changes of α_1 and β_2, (a2) the equilibrium points $Q_\pm$ under the changes of α_1 and β_2, (b1) the equilibrium point Q_0 under the changes of α_2 and β_1, (b2) the equilibrium point $Q_\pm$ under the changes of α_2 and β_1.

bifurcation diagrams created with the local maximum for variable x about the parameters α_1 and α_2 are drawn in **Fig. 4** (a1) and (b1) respectively, where the other parameters are taken from normalized typical parameters (11). Correspondingly, the first two Lyapunov exponents about the parameters α_1 and α_2 computed with Wolf's method [39] are drawn in **Fig. 4** (a2) and (b2) respectively, where a set of unique initial values $(x(0), y(0), z(0), w(0)) = (0, 0, -1, 0)$ is selected.

Observed from **Fig. 4** (a1) and (a2), multiple bifurcation behaviors can be found with the increase of α_1 and some main conclusions can be drawn. For the initial values (0, 0, −1, 0) and (0, 0, 1, 0), the system develops from coexisting point attractors to coexisting limit cycles of period-1, and then evolves into coexisting single-scroll attractors of chaos through coexisting period-doubling bifurcation models. Bridged by a broad window of coexisting limit cycles of period-3, the system turns into double-scroll attractor of chaos. Such an interesting crisis scenario triggered by coexisting limit cycles of period-3 is consistent with the related report from literature [26]. During the interval of double-scroll chaotic oscillation, boundary crisis occurs many times, which are triggered by a series of tangent bifurcations with double-band periodic oscillation of period-7, period-5 and period-3. When $\alpha_1 > 9.55$, the limit cycle with large amplitude emerges. For the initial values (−1, 0, 1, −1) and (1, 0, −1, 1) which are close to the two stable equilibrium points

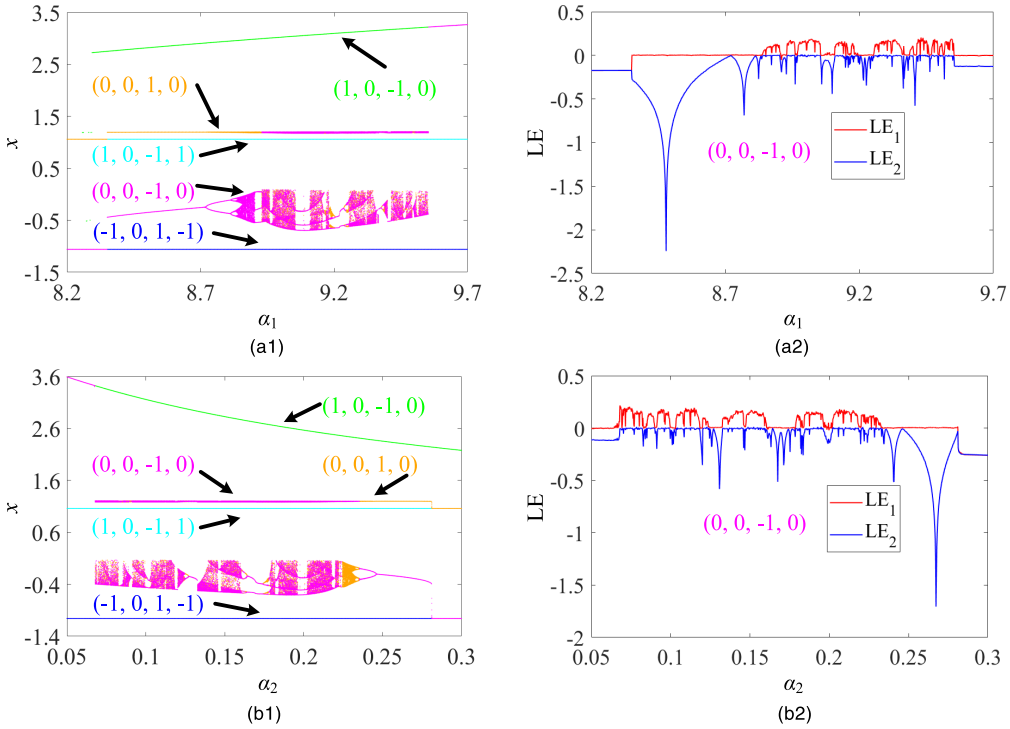

FIGURE 4. Multiple dynamical behaviors of model (5). (a1) bifurcation diagrams for x about α_1, (a2) Lyapunov exponent spectra about α_1, (b1) bifurcation diagrams for x about α_2, (b2) Lyapunov exponent spectra about α_2.

$Q_\pm$, left or right point attractor in wide intervals can be triggered. For the initial value $(1, 0, -1, 0)$ which is far from $Q_\pm$, the limit cycle with large amplitude can be triggered. The similar dynamical behaviors with the increase of α_2 can be observed from **Fig. 4** (b1) and (b2), but this process is inverted compared with **Fig. 4** (a1) and (a2).

For better observing of the above multiple bifurcation behaviors, the coexisting multiple attractors with a series of representative values for α_1 are simulated numerically, as shown in **Fig. 5**. It should be noted that these phase portraits of the limit cycle with large amplitude are drawn partly for clarity. As far as the coexisting oscillation behaviors with small amplitude are concerned, **Fig. 5** (a), (b) and (c) express the evolution of period-doubling bifurcation path to chaos, and **Fig. 5** (e) presents double-scroll attractor of chaos while **Fig. 5** (d) expresses the interesting transitional characteristics from coexisting single-scroll attractors of chaos to double-scroll one as coexisting limit cycles of period-3, and **Fig. 5** (f), (g) and (h) express double-band limit cycles which are successively sampled from the periodic windows of period-7, period-5 and period-3. Furthermore, for these oscillation behaviors with small amplitude in **Fig. 5** and **Fig. 2** (a), the expanding capability of the attractors is strengthened gradually and the contraction capacity is weakened gradually with the increasing of parameter value α_1. During this process, single-band oscillation evolves into double-band oscillation. And the dominant oscillation shape develops from scroll to tendon for the double-scroll attractors, which can be represented by **Fig. 5** (e) and **Fig. 2** (a). Accordingly, the maximum value for the real parts of four eigenvalues in **Fig. 3** (a1) and (a2) increases gradually with the increasing of parameter value α_1, which can be regarded as one explanation for the above repellent and attractive dynamics. Thus, for the double-band limit cycles of period-7, period-5 and period-3 in **Fig. 5** (f), (g) and (h), the reduction for the number of periodic orbits around the equilibrium points $Q_\pm$ is the result of the weakening of attractive ability from $Q_\pm$.

B. TWO-PARAMETER DYNAMICAL BEHAVIORS

Two-parameter bifurcation diagram and dynamical map can reflect the dynamical behaviors of model (5) visually and adequately. When the parameters α_1 and β_2 change in accordance with the value ranges of **Fig. 3** (a1) and (a2), the two-parameter bifurcation diagram and dynamical map [40] are plotted by **Fig. 6** (a1) and (a2) respectively. Similarly, when the parameters α_2 and β_1 change in accordance with the value ranges of **Fig. 3** (b1) and (b2), the numerical results are plotted by **Fig. 6** (b1) and (b2) respectively. For the two-parameter bifurcation diagrams (a1) and (b1) described with the periodicities to variable x, the codes P0, CH and LP represent the point attractor, chaotic attractor and the limit cycle with large amplitude respectively. Note here that the initial values in the four graphs of **Fig. 6** are $(x(0), y(0), z(0), w(0)) = (0, 0, -1, 0)$. Compared with the bifurcation diagrams triggered by the magenta initial condition and the corresponding largest Lyapunov exponent spectra in **Fig. 4**, **Fig. 6** show high consistency at $\beta_2 = 9.9275$ for (a1, a2) and $\beta_1 = 99.275$ for (b1, b2).

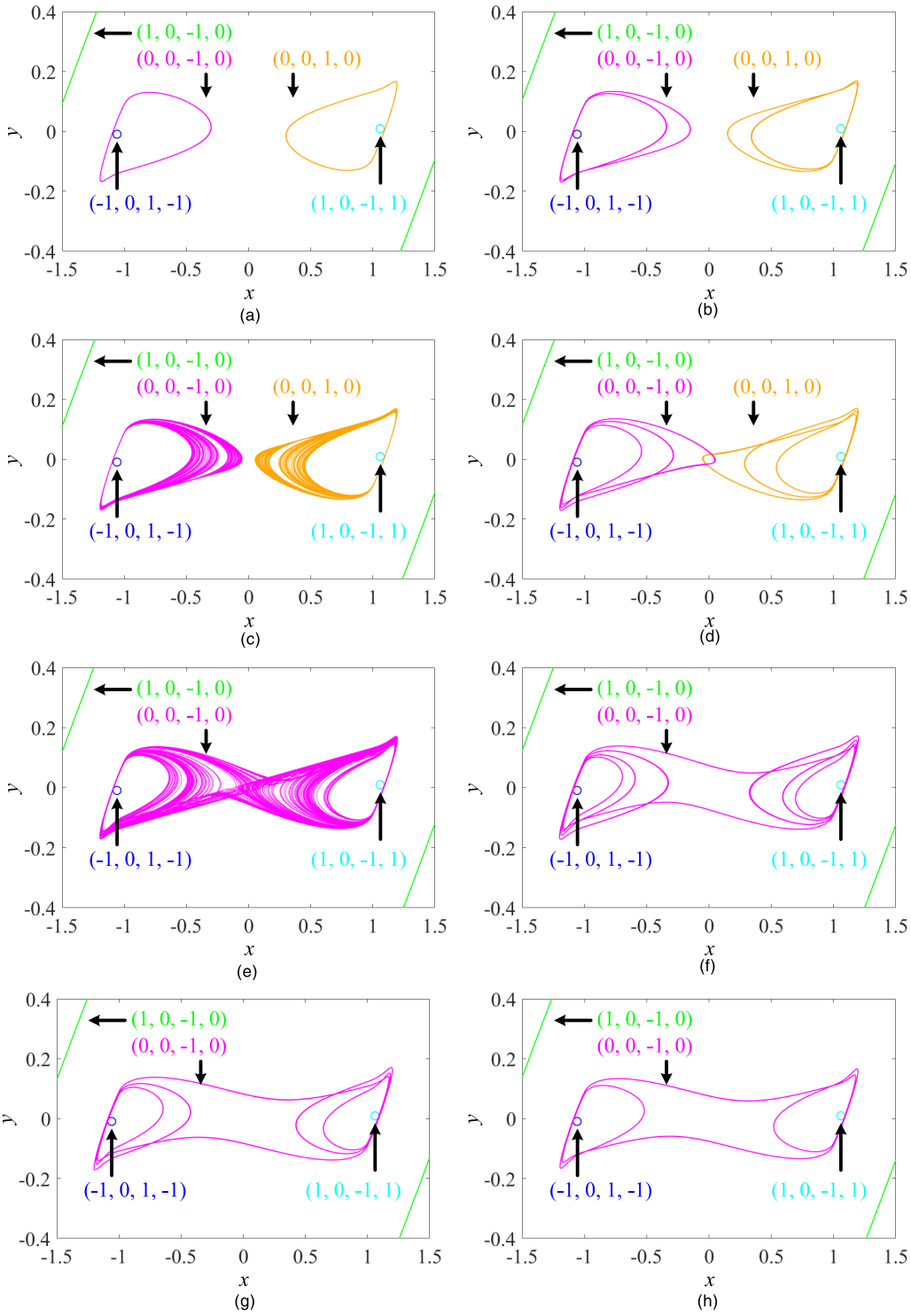

FIGURE 5. Coexisting multiple attractors with a series of representative values for α_1. (a) $\alpha_1 = 8.6$, (b) $\alpha_1 = 8.77$, (c) $\alpha_1 = 8.85$, (d) $\alpha_1 = 8.915$, (e) $\alpha_1 = 9$, (f) $\alpha_1 = 9.08$, (g) $\alpha_1 = 9.216$, (h) $\alpha_1 = 9.408$.

Deserved to be mentioned, the hyperchaos phenomenon is not discovered in this new fourth order Chua's circuit. Some features for the three kinds of fourth order Chua's circuits in [27], [28] and this article are summarized in TABLE 1. Obviously, the disappearance of the hyperchaos phenomenon and the emergence of coexisting point attractors for the circuit in this article are two clear dynamical features different from the circuit in [28]. Furthermore, compared with the classical five-segment piecewise Chua's diode, the introduction of three-segment piecewise Chua's diode for fourth order Chua's

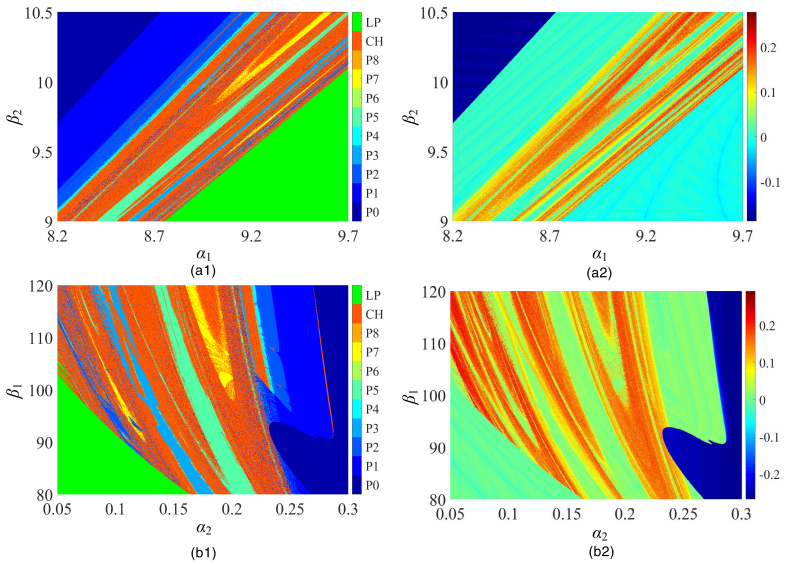

FIGURE 6. Two-parameter bifurcation diagrams and dynamical maps described with the largest Lyapunov exponent for model (5). (a1) bifurcation diagram on α_1-β_2 parameter plane, (a2) dynamical map on α_1-β_2 parameter plane, (b1) bifurcation diagram on α_2-β_1 parameter plane, (b2) dynamical map on α_2-β_1 parameter plane.

TABLE 1. Some features for three kinds of fourth order Chua's circuits.

Literature sources	Number of inductances	Number of capacitances	Number of op amps	Nonlinear characteristic	Dynamical behaviors
[27]	1	3	2	Five-segment piecewise	Period and chaos
[28]	2	2	2	Three-segment piecewise	Period, chaos and hyperchaos
This article	2	2	1	Three-segment piecewise	Point attractor, period and chaos

circuits doesn't mean there will be no hyperchaotic behavior, and this also doesn't mean that point attractor will certainly emerge. Clearly these dynamical behaviors depend not only on the nonlinear characteristic of Chua's diode but also on the circuit structure and the corresponding parameters.

C. ATTRACTION BASINS ANALYSIS

For better analysis of the coexisting behaviors for multiple attractors, the local attraction basins are introduced. When the normalized typical parameters (11) are adopted, the local attraction basins in the $x(0)$ $-w(0)$ plane with $y(0) = 0$ and $z(0) = -1$ are drawn, as shown by **Fig. 7**. (a). And when the parameter α_1 decreases from 9.482759 to 8.85, the corresponding local attraction basins are given by **Fig. 7**. (b). Compared with the phase portraits in **Fig. 2** and **Fig. 5** (c) which have the same parameters values separately, **Fig. 7**. (a) and (b) present symmetrical coexisting behaviors further and the colors of the coordinate points have the same meaning of dynamics as those used in **Fig. 2** and **Fig. 5** (c) except for the red color used to denote the double-scroll chaotic oscillatory behavior. Obviously, for the local attraction basins, the initial values near the coordinate values of the two stable equilibrium points $Q_{\pm}$ introduce the system to the corresponding point attractors. In **Fig. 7**. (b), symmetrical and intertwined fractal structures can be observed, which confirms that the two coexisting point attractors and two coexisting single-scroll chaotic attractors presented in **Fig. 5** (c) are highly sensitive to the initial values.

IV. DUAL-MODE EXPERIMENTAL VERIFICATIONS BY ANALOG AND DIGITAL CIRCUITS

For verifying the above dynamical behaviors, the dual-mode experiments of analog and digital circuits are carried out. The photographs of two experimental scenarios are expressed by **Fig. 8** (a) and (b) respectively, among which all the printed circuit boards (PCBs) are designed by the authors of this article. In the most PCBs, the large grounding plane can not only restrain the ground bounce noise from the ground itself but also weaken the mutual inductance coupling noise from the parallel lines. The digital oscilloscope DSO7054B is used to capture the various coexisting attractors. For clarity, the point attractors are captured in ordinary resolution model while the other attractors are captured in high resolution model.

According to **Fig. 1**, the analog circuit shown by **Fig. 8** (a) is designed and fabricated with modular design approach. Here a main circuit and two small inductance support board circuits are installed on a large support board with three self-locking power switches. During the experiments, a piece of AD711KNZ op amp chip is selected and powered with ± 15 V DC. When $R_a = 1.8$ kΩ, $R_b = R_c = 20$ kΩ, $R_1 = 1.9$ kΩ, $R_2 = 2$ Ω, $R_3 = 50$ kΩ,

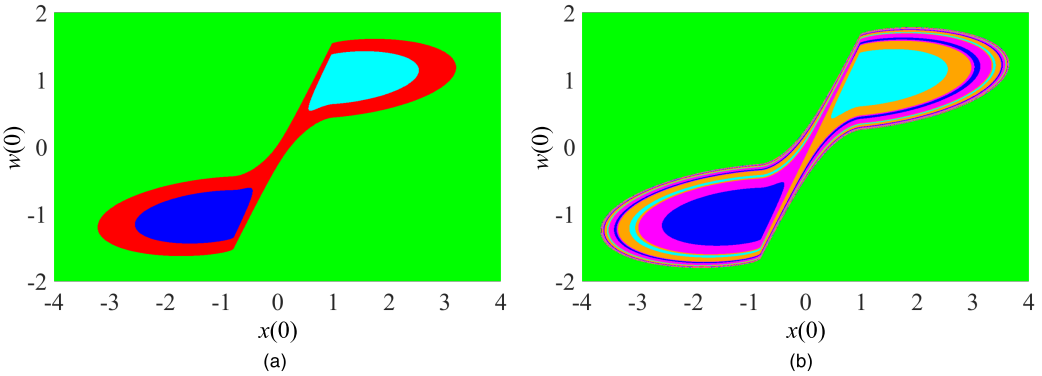

FIGURE 7. Local attraction basins on $x(0)-w(0)$ plane with $y(0)=0$ and $z(0)=-1$. (a) under the normalized typical parameters (11), (b) α_1 decreases to 8.85 on the basis of parameters (11).

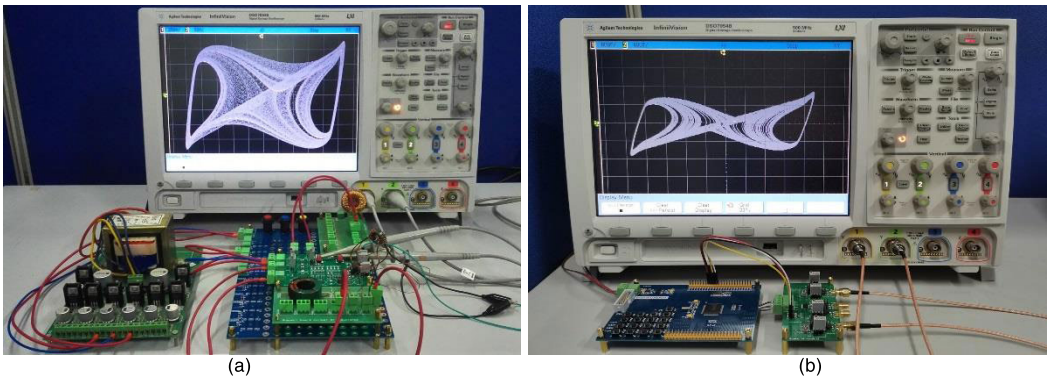

FIGURE 8. The photographs of two experimental scenarios. (a) analog circuit, (b) digital circuit.

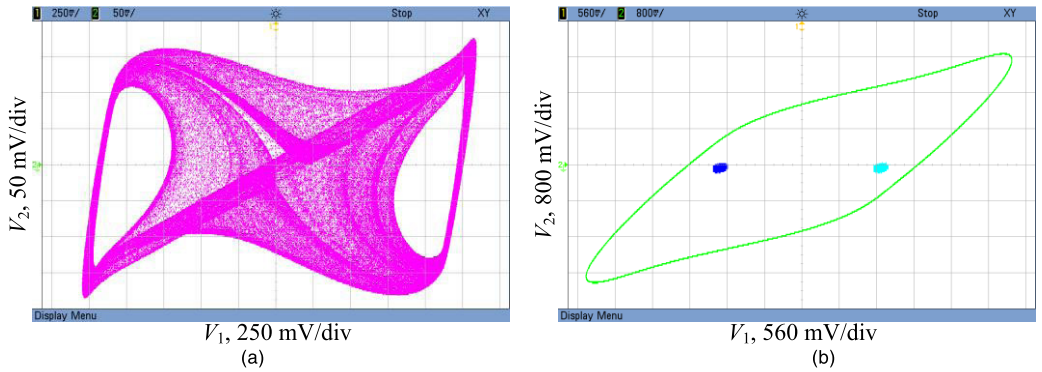

FIGURE 9. The experiment results by analog circuit. (a) the double-scroll attractor of chaos, (b) the limit cycle with large amplitude, left-right point attractors.

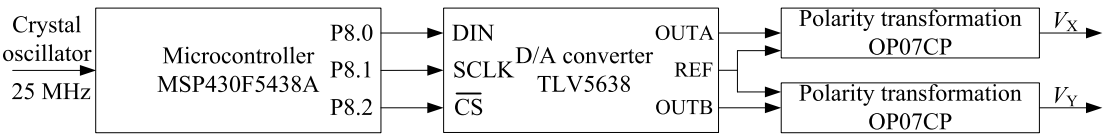

FIGURE 10. The block diagram of digital circuit experiment system.

$C_1 = 5.6$ nF, $C_2 = 53$ nF, $L_1 = 2.2$ mH, $L_2 = 22$ mH, these coexisting double-scroll attractor of chaos, limit cycle with large amplitude, left-right point attractors can be triggered through switching on and switching off the power supplies for many times, as given by **Fig. 9**. It should be mentioned that the capacitance C_1 is achieved by connecting several fixed capacitors and a small adjustable capacitor in parallel with a dash of measuring errors. Obviously, the experiment results are roughly identical to the simulation results in **Fig. 2**. Although there are some deviations between this set of actual parameters and the typical parameters given in **Section II B**, these results confirm the basic realizability of the new fourth order Chua's circuit physically.

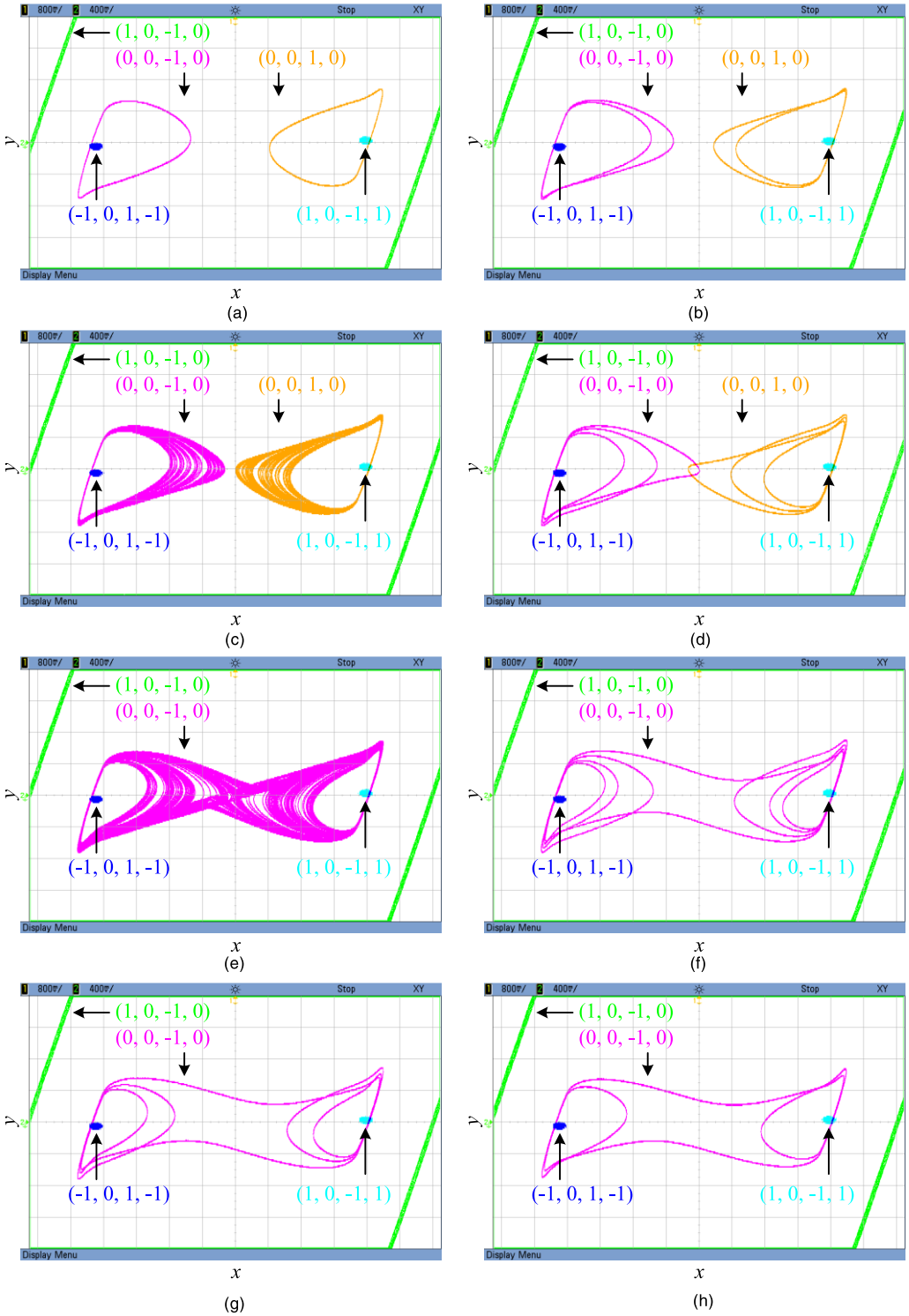

FIGURE 11. The experiment results with a series of representative values for α_1 by digital circuit. (a) $\alpha_1 = 8.75$, (b) $\alpha_1 = 8.94$, (c) $\alpha_1 = 9.04$, (d) $\alpha_1 = 9.1$, (e) $\alpha_1 = 9.2$, (f) $\alpha_1 = 9.28$, (g) $\alpha_1 = 9.41$, (h) $\alpha_1 = 9.62$.

It is widely acknowledged that the symmetry of mathematical model determines the existence of symmetric paired coexisting attractors for chaotic system in theory [41]. However, the corresponding actual analog circuit may not be very symmetric, which will affect the experiment results especially for left-right coexisting periodic or chaotic oscillation behaviors with small amplitude. Because of the discrete, parasitic and asymmetric properties [42] of the actual component parameters, it is very difficult to obtain the coexisting multiple attractors similar to **Fig. 5** through this analog circuit with a lot of experiments. For better verifying of the multiple bifurcation behaviors about normalized model (5) with the

change of α_1 by hardware circuit, an experimental scheme with digital circuit is devised and implemented, as given previously in **Fig. 8** (b). In this scheme, the 16-bit microcontroller MSP430F5438A with low power consumption is used to generate the digital chaos signal and the two-channel 12-bit digital to analog converter TLV5638 is used to complete the signal conversion, as shown by **Fig. 10**. Here the two circuits of voltage transformation from unipolarity to bipolarity are designed on the basis of the application report numbered SLAA113A from Texas Instruments Incorporated [43].

Different from the uncertain attractors triggered by the random initial states of dynamic components in multi-stable analog circuit, the various certain attractors can be achieved respectively in microcontroller digital circuit by setting corresponding initial values of state variables in program code. Meanwhile the engineering application for digital circuit is more reliably realized compared with that for analog circuit. Hence this digitized implementation approach is meaningful in both rigorous scientific demonstration and potential engineering application for high order nonlinear multi-stable system.

Based on a special third order Runge-Kutta method, a group of difference equations can be achieved from the ordinary differential equations (5), as shown by

$$\begin{cases} x_{n+1} = x_n + h(k_{x1} + 4k_{x2} + k_{x3})/6 \\ y_{n+1} = y_n + h(k_{y1} + 4k_{y2} + k_{y3})/6 \\ z_{n+1} = z_n + h(k_{z1} + 4k_{z2} + k_{z3})/6 \\ w_{n+1} = w_n + h(k_{w1} + 4k_{w2} + k_{w3})/6 \end{cases} \tag{14}$$

Here h represents the time step while (x_n, y_n, z_n, w_n) and $(x_{n+1}, y_{n+1}, z_{n+1}, w_{n+1})$ represent the current point and the next point respectively. The calculation formulas for the slopes of the current point and the two forecast points are expressed as

$$N = m_b x_n + \frac{1}{2}(m_a - m_b)(|x_n + 1| - |x_n - 1|) \tag{15}$$

$$\begin{cases} k_{x1} = \alpha_1 [z_n - N] \\ k_{y1} = -\alpha_2 y_n - z_n - w_n \\ k_{z1} = \beta_1 (y_n - x_n - z_n) \\ k_{w1} = \beta_2 (y_n - \alpha_3 w_n) \end{cases} \tag{16}$$

$$\begin{cases} k_{x2} = \alpha_1 [(z_n + 0.5hk_{z1}) - N] \\ k_{y2} = -\alpha_2(y_n + 0.5hk_{y1}) - (z_n + 0.5hk_{z1}) \\ \qquad\qquad -(w_n + 0.5hk_{w1}) \\ k_{z2} = \beta_1 \left[(y_n + 0.5hk_{y1}) - (x_n + 0.5hk_{x1}) \right. \\ \qquad\qquad \left. -(z_n + 0.5hk_{z1})\right] \\ k_{w2} = \beta_2 \left[(y_n + 0.5hk_{y1}) - \alpha_3(w_n + 0.5hk_{w1})\right] \end{cases} \tag{17}$$

$$\begin{cases} k_{x3} = \alpha_1 [(z_n + hk_{z2}) - N] \\ k_{y3} = -\alpha_2(y_n + hk_{y2}) - (z_n + hk_{z2}) - (w_n + hk_{w2}) \\ k_{z3} = \beta_1 \left[(y_n + hk_{y2}) - (x_n + hk_{x2}) - (z_n + hk_{z2})\right] \\ k_{w3} = \beta_2 \left[(y_n + hk_{y2}) - \alpha_3(w_n + hk_{w2})\right] \end{cases} \tag{18}$$

where the nonlinear term N is considered as the function of the current point and not affected by the two forecast points in the calculations.

According to the above computational methods, a series of programs with the change of α_1 based on the normalized typical parameters (11) are designed with C language, where the several initial values corresponding to **Fig. 5** and the unified time step $h = 0.005$ are introduced. Driven by the crystal oscillator with 25 MHz clock frequency, the microcontroller MSP430F5438A performs these programs respectively. **Fig. 11** provides these corresponding experiment results exported from the TLV5638 PCB circuit with bipolar voltage outputs. It can be observed that these experiment results are highly consistent with those simulation results shown by **Fig. 5** under the conditions of appropriate reductions for α_1. Thus, the multiple dynamical behaviors in **Section III** are confirmed by circuit experiments.

V. CONCLUSION

In this article, a succinct fourth order Chua's circuit is proposed based on a traditional fourth order Chua's circuit. From the circuit structure, the positive resistance takes the place of the negative one in the traditional fourth order Chua's circuit, thereby reducing the number of op amps and simplifying the circuit. The experimental verification by analog circuit confirms the realizability of the new fourth order Chua's circuit physically. From the stability of equilibrium points, one unstable saddle-focus point of index 1 and two stable node-focus points are discovered in the two-parameter planes based on the normalized typical parameters. From the dynamical behaviors, coexisting bifurcation models, multiple attractors and the corresponding attraction basins are revealed by a series of numerical computation. It is interesting that the coexisting limit cycles of period-3 build a bridge between the coexisting single-scroll attractors of chaos and the double-scroll one. During the interval of double-scroll chaotic oscillation, the crisis scenarios triggered by a series of tangent bifurcations with double-band periodic oscillation of period-7, period-5 and period-3 appear successively. The experimental verification by digital circuit is carried out on the 16-bit microcontroller MSP430F5438A, and the corresponding experiment results confirm those simulated dynamical behaviors completely. Moreover, the digital and programmed realization way offers the opportunity for the engineering application based on chaos [26], [44].

REFERENCES

[1] J. Sun, Y. Wu, G. Cui, and Y. Wang, "Finite-time real combination synchronization of three complex-variable chaotic systems with unknown parameters via sliding mode control," *Nonlinear Dyn.*, vol. 88, no. 3, pp. 1677–1690, May 2017.
[2] M. Chen, Q. Xu, Y. Lin, and B. Bao, "Multistability induced by two symmetric stable node-foci in modified canonical Chua's circuit," *Nonlinear Dyn.*, vol. 87, no. 2, pp. 789–802, Jan. 2017.
[3] C. Li, X. Wang, and G. Chen, "Diagnosing multistability by offset boosting," *Nonlinear Dyn.*, vol. 90, no. 2, pp. 1335–1341, Oct. 2017.
[4] Y. Zhang, Z. Liu, H. Wu, S. Chen, and B. Bao, "Extreme multistability in memristive hyper-jerk system and stability mechanism analysis using dimensionality reduction model," *Eur. Phys. J. Special Topics*, vol. 228, no. 10, pp. 1995–2009, Oct. 2019.

[5] X. Zhang and Z. Li, "Hidden extreme multistability in a novel 4D fractional-order chaotic system," *Int. J. Non-Linear Mech.*, vol. 111, pp. 14–27, May 2019.
[6] J. Sun, X. Zhao, J. Fang, and Y. Wang, "Autonomous memristor chaotic systems of infinite chaotic attractors and circuitry realization," *Nonlinear Dyn.*, vol. 94, no. 4, pp. 2879–2887, Dec. 2018.
[7] Q. Lai, G. Xu, and H. Pei, "Analysis and control of multiple attractors in Sprott B system," *Chaos, Solitons Fractals*, vol. 123, pp. 192–200, Jun. 2019.
[8] Q. Lai, C. Chen, X.-W. Zhao, J. Kengne, and C. Volos, "Constructing chaotic system with multiple coexisting attractors," *IEEE Access*, vol. 7, pp. 24051–24056, Feb. 2019.
[9] T. Matsumoto, "A chaotic attractor from Chua's circuit," *IEEE Trans. Circuits Syst.*, vol. CS-31, no. 12, pp. 1055–1058, Dec. 1984.
[10] M. P. Kennedy, "Three steps to chaos. II. A Chua's circuit primer," *IEEE Trans. Circuits Syst. I, Fundam. Theory Appl.*, vol. 40, no. 10, pp. 657–674, Oct. 1993.
[11] T. Matsumoto, L. O. Chua, and M. Komuro, "The double scroll," *IEEE Trans. Circuits Syst.*, vol. CAS-32, no. 8, pp. 797–818, Aug. 1985.
[12] M. P. Kennedy, "Robust OP amp realization of Chua's circuit," *Frequenz*, vol. 46, nos. 3–4, pp. 66–80, Jan. 1992.
[13] Z. Y. Chen, X. F. Zhang, and Q. S. Bi, "Bursting phenomenon and the bifurcation mechanism in generalized Chua's circuit," *Acta Phys. Sinica*, vol. 59, no. 4, pp. 2326–2333, Apr. 2010.
[14] G. A. Leonov, N. V. Kuznetsov, and V. I. Vagaitsev, "Localization of hidden Chua's attractors," *Phys. Lett. A*, vol. 375, no. 23, pp. 2230–2233, Jun. 2011.
[15] Q. Li, H. Zeng, and X.-S. Yang, "On hidden twin attractors and bifurcation in the Chua's circuit," *Nonlinear Dyn.*, vol. 77, nos. 1–2, pp. 255–266, Jul. 2014.
[16] B. C. Bao, Q. D. Li, N. Wang, and Q. Xu, "Multistability in Chua's circuit with two stable node-foci," *Chaos*, vol. 26, no. 4, pp. 043111-1–043111-9, Apr. 2016.
[17] B. C. Bao, H. G. Wu, L. Xu, M. Chen, and W. Hu, "Coexistence of multiple attractors in an active diode pair based Chua's circuit," *Int. J. Bifurcation Chaos*, vol. 28, no. 2, pp. 1850019-1–1850019-13, Feb. 2018.
[18] S. Yu, W. K. S. Tang, and G. Chen, "Generation OF n × m-scroll attractors under a Chua-circuit framework," *Int. J. Bifurcation Chaos*, vol. 17, no. 11, pp. 3951–3964, Nov. 2007.
[19] C. H. Wang, H. Xu, and F. Yu, "A novel approach for constructing high-order Chua's circuit with multi-directional multi-scroll chaotic attractors," *Int. J. Bifurcation Chaos*, vol. 23, no. 2, pp. 1350022-1–1350022-10, Feb. 2013.
[20] X. X. Ai, K. H. Sun, S. B. He, and H. H. Wang, "Design of grid multiscroll chaotic attractors via transformations," *Int. J. Bifurcation Chaos*, vol. 25, no. 10, pp. 1530027-1–1530027-12, Sep. 2015.
[21] Y. Liu and S. X. Guo, "Generation and dynamics analysis of N-scrolls existence in new translation-type chaotic systems," *Chaos*, vol. 26, no. 11, pp. 113114-1–113114-12, Nov. 2016.
[22] Y. Liu, H. H.-C. Iu, H. Li, and X. Zhang, "Bounded orbits and multiple scroll coexisting attractors in a dual system of Chua system," *IEEE Access*, vol. 8, pp. 147907–147918, Aug. 2020.
[23] Z. Li, M. Ma, M. Wang, and Y. Zeng, "Realization of current-mode SC-CNN-based Chua's circuit," *AEU-Int. J. Electron. Commun.*, vol. 71, pp. 21–29, Jan. 2017.
[24] B. Bao, N. Wang, M. Chen, Q. Xu, and J. Wang, "Inductor-free simplified Chua's circuit only using two-op-amp-based realization," *Nonlinear Dyn.*, vol. 84, no. 2, pp. 511–525, Apr. 2016.
[25] T. Banerjee, "Single amplifier biquad based inductor-free Chua's circuit," *Nonlinear Dyn.*, vol. 68, no. 4, pp. 565–573, Jun. 2012.
[26] L. Zhu, M. Pan, and X. Qiao, "A chaotic circuit under a new classification framework of inductorless Chua's circuits," *Circuit World*, vol. 45, no. 4, pp. 208–220, Nov. 2019.
[27] F. Yu, H. Shen, L. Liu, Z. Zhang, Y. Huang, B. He, S. Cai, Y. Song, B. Yin, S. Du, and Q. Xu, "CCII and FPGA realization: A multistable modified fourth-order autonomous Chua's chaotic system with coexisting multiple attractors," *Complexity*, vol. 2020, Mar. 2020, Art. no. 5212601.
[28] K. Thamilmaran, M. Lakshmanan, and A. Venkatesan, "Hyperchaos in a modified canonical Chua's circuit," *Int. J. Bifurcation Chaos*, vol. 14, no. 1, pp. 221–243, Jan. 2004.
[29] Y. Ji and Q. S. Bi, "Bifurcation analysis of slow-fast behavior in modified Chua's circuit," *Acta Phys. Sinica*, vol. 61, no. 1, pp. 010202-1–010202-6, Jan. 2012.
[30] N. Wang, G. Zhang, and H. Bao, "A simple autonomous chaotic circuit with dead-zone nonlinearity," *IEEE Trans. Circuits Syst. II, Exp. Briefs*, vol. 67, no. 12, pp. 3502–3506, Dec. 2020, doi: 10.1109/TCSII.2020.3005726.
[31] Z. Hua, Y. Zhou, and B. Bao, "Two-dimensional sine chaotification system with hardware implementation," *IEEE Trans. Ind. Informat.*, vol. 16, no. 2, pp. 887–897, Feb. 2020.
[32] Z. Gu, C. Li, H. H. C. Iu, F. Min, and Y. Zhao, "Constructing hyperchaotic attractors of conditional symmetry," *Eur. Phys. J. B*, vol. 92, no. 10, Oct. 2019, Art. no. 100165.
[33] X. Zhang, C. B. Li, Y. D. Chen, H. H. C. Iu, and T. F. Lei, "A memristive chaotic oscillator with controllable amplitude and frequency," *Chaos, Solitons Fractals*, vol. 139, pp. 1–10, Oct. 2020.
[34] Q. Lai, Z. Wan, P. D. K. Kuate, and H. Fotsin, "Coexisting attractors, circuit implementation and synchronization control of a new chaotic system evolved from the simplest memristor chaotic circuit," *Commun. Nonlinear Sci. Numer. Simul.*, vol. 89, Oct. 2020, Art. no. 105341.
[35] A. Arulgnanam, K. Thamilmaran, and M. Daniel, "Chaotic dynamics with high complexity in a simplified new nonautonomous nonlinear electronic circuit," *Chaos, Solitons Fractals*, vol. 42, no. 4, pp. 2246–2253, Nov. 2009.
[36] J. Sun, G. Han, Z. Zeng, and Y. Wang, "Memristor-based neural network circuit of full-function pavlov associative memory with time delay and variable learning rate," *IEEE Trans. Cybern.*, vol. 50, no. 7, pp. 2935–2945, Jul. 2020.
[37] C. Li, W. J.-C. Thio, J. C. Sprott, H. H.-C. Iu, and Y. Xu, "Constructing infinitely many attractors in a programmable chaotic circuit," *IEEE Access*, vol. 6, pp. 29003–29012, Apr. 2018.
[38] K. Sun and J. C. Sprott, "Dynamics of a simplified lorenz system," *Int. J. Bifurcation Chaos*, vol. 19, no. 04, pp. 1357–1366, Apr. 2009.
[39] A. Wolf, J. B. Swift, H. L. Swinney, and J. A. Vastano, "Determining Lyapunov exponents from a time series," *Phys. D, Nonlinear Phenomena*, vol. 16, no. 3, pp. 285–317, Jul. 1985.
[40] Y. Zhang, Z. Liu, H. Wu, S. Chen, and B. Bao, "Two-memristor-based chaotic system and its extreme multistability reconstitution via dimensionality reduction analysis," *Chaos, Solitons Fractals*, vol. 127, pp. 354–363, Oct. 2019.
[41] Y. Liu and H. H.-C. Iu, "Antimonotonicity, chaos and multidirectional scroll attractor in autonomous ODEs chaotic system," *IEEE Access*, vol. 8, pp. 77171–77178, Apr. 2020.
[42] Y. Ye, J. Zhou, Q. Xu, M. Chen, and H. Wu, "Parallel-type asymmetric memristive diode-bridge emulator and its induced asymmetric attractor," *IEEE Access*, vol. 8, pp. 156299–156307, Aug. 2020.
[43] *Texas Instruments Incorporated, USA*. Accessed: May 2015. [Online]. Available: https://www.ti.com/lit/pdf/slaa113
[44] C. Li, Y. Xu, G. Chen, Y. Liu, and J. Zheng, "Conditional symmetry: Bond for attractor growing," *Nonlinear Dyn.*, vol. 95, no. 2, pp. 1245–1256, Jan. 2019.

LEI ZHU was born in 1979. He received the B.S. degree from Yangzhou University, Yangzhou, China, in 2002, and the M.S. degree from Yanshan University, Qinhuangdao, China, in 2006. He is currently pursuing the Ph.D. degree in communication and information systems with the Nanjing University of Aeronautics and Astronautics, Nanjing, China.

He is also an Associate Professor with the School of Electrical and Information Engineering, Jiangsu University of Technology, Changzhou, China. His research interest includes nonlinear circuits and systems.

MINGHAI PAN was born in 1962. He received the M.S. and Ph.D. degrees from the Harbin Institute of Technology, in 1988 and 2000, respectively. He is currently a Professor and a Ph.D. Supervisor with the College of Electronic and Information Engineering, Nanjing University of Aeronautics and Astronautics. His research interests include radar system design, RF simulation, and radar signal processing.